Stochastic Properties of Ca^{2+} Release of Inositol 1,4,5-Trisphosphate Receptor Clusters

Jian-Wei Shuai and Peter Jung
Department of Physics and Astronomy and Institute for Quantitative Biology, Ohio University, Athens, Ohio 45701 USA

ABSTRACT Intracellular Ca^{2+} release is controlled by inositol 1,4,5-trisphosphate (IP_3) receptors or ryanodine receptors. These receptors are typically distributed in clusters with several or tens of channels. The random opening and closing of these channels introduces stochasticity into the elementary calcium release mechanism. Stochastic release events have been experimentally observed in a variety of cell types and have been termed sparks and puffs. We put forward a stochastic version of the Li-Rinzel model (the deactivation binding process is described by a Markovian scheme) and a computationally more efficient Langevin approach to model the stochastic Ca^{2+} oscillation of single clusters. Statistical properties such as Ca^{2+} puff amplitudes, lifetimes, and interpuff intervals are studied with both models and compared with experimental observations. For clusters with tens of channels, a simply decaying amplitude distribution is typically observed at low IP_3 concentration, while a single peak distribution appears at high IP_3 concentration.

INTRODUCTION

Intracellular calcium signals were first observed in medaka eggs and later on in various other cell types (Cornell-Bell et al., 1990; Bezprovanny et al., 1991). Intracellular Ca^{2+} signals are due to release of Ca^{2+} from intracellular stores such as the endoplasmic reticulum (ER) or the sarcoplasmic reticulum (SR) through inositol 1,4,5-trisphosphate receptor channels (IP_3R) or ryanodine receptor channels (RyR). Cytosolic Ca^{2+} signals in intact cells can display spatially and temporally complex patterns (Cornell-Bell et al., 1990; Newman and Zahs, 1997; Harris-White et al., 1998). They can act as second messengers in living cells to regulate multiple cellular functions such as neurotransmitter release, synaptic plasticity, gene expression, and cell death (Golovina and Blaustein, 1997; Koninck and Schulman, 1998; Allen et al., 2000).

Recently, high-resolution recordings enable us to investigate elementary intracellular Ca^{2+} release events. It has been observed that the Ca^{2+} release channels are spatially organized in clusters. The collective opening and closing of several calcium release channels in a cluster causes Ca^{2+} puffs or sparks observed in experiments (Cheng et al., 1993; Callamaras et al., 1998; Melamed-Book et al., 1999; Gonzalez et al., 2000; Mak et al., 2001). Ca^{2+} blips arising from the opening of single release channels have also been observed in experiments (Bootman et al., 1997; Lipp and Niggli, 1998; Sun et al., 1998). Typically, puffs remain spatially restricted at a low concentration of IP_3 stimulus. At high levels of $[IP_3]$, neighboring clusters become functionally coupled by Ca^{2+} diffusion and Ca^{2+}-induced Ca^{2+} release (Bezprovanny et al., 1991) to support global Ca^{2+} waves that propagate in a saltatory manner throughout the cell. Therefore, Ca^{2+} puffs serve as elementary building blocks of global Ca^{2+} waves. Moreover, puffs can arise spontaneously before a wave is initiated and can act as the triggers to initiate waves (Bootman et al., 1997). Calcium puffs provide a unique window on the dynamics of local calcium release.

Observations of Ca^{2+} signals of differing magnitudes suggested a hierarchy of calcium signaling events, with the smaller blips representing fundamental events involving opening of single IP_3R and the larger puffs being elementary events resulting from the opening of small groups of IP_3Rs (Lipp and Niggli, 1998; Bootman et al., 1997). Improved spatial and temporal resolutions in recordings reveal that Ca^{2+} release is not functionally quantized into discrete, stereotypical events of clearly separable magnitude. Instead, the amounts of calcium liberated during different events show a continuous distribution over a wide range, even when monitored from a single site (Bootman et al., 1997; Sun et al., 1998; Thomas et al., 1998; Callamaras and Parker, 2000; Marchant and Parker, 2001; Haak et al., 2001). There is not a clear distinction between fundamental and elementary events. Experimental data suggest that the localized calcium release varies in a continuous fashion due to stochastic variation in both numbers of channels recruited and durations of channel openings.

The knowledge about the calcium release mechanism is directly related to the distribution of calcium-puff amplitudes. Generally, the morphology, i.e., spatial extent, duration and amplitude, of puffs or sparks can be used to infer the release flux and the number of release channels involved locally in release (Bootman et al., 1997; Smith et al., 1998; Sun et al., 1998; Thomas et al., 1998; Jiang et al., 1999; Callamaras and Parker, 2000; Marchant and Parker, 2001). The experimental determination of the puff amplitudes is difficult at small amplitudes because the apparatus response function and cutoff can modify the actual amplitudes (Pra-

Submitted October 2, 2001, and accepted for publication February 19, 2002.

Address reprint requests to Jian-Wei Shuai, Department of Physics and Astronomy, Clippinger Research Laboratories, Room 252A, Ohio University, Athens, OH 45701. Tel.: 740-593-9434; Fax: 740-593-0433; E-mail: shuai@helios.phy.ohiou.edu.

0006-3495/02/07/87/11 $2.00

tusevich and Balke, 1996; Izu et al., 1998; Cheng et al., 1999; Rios et al., 2001). Experimentally, it is not obvious which aspects of Ca^{2+} puffs are originally determined by the dynamics of the Ca^{2+} channels, which properties are determined by the diffusion and Ca^{2+} binding kinetics of both the intrinsic binding sites in the fiber and the Ca^{2+} indicator dye, and which properties are induced from the measurement of confocal line scan image.

It has been shown that the experimental amplitude distributions are far from the true distribution of puff amplitudes due to various factors in the experiment (Pratusevich and Balke, 1996; Smith et al., 1998; Izu et al., 1998; Jiang et al., 1999). Cheng et al. (1999) suggested that the original calcium puffs should have a monotonically decreasing amplitude distribution, regardless of whether the underlying events are stereotyped. In contrast, Rios et al. (2001) reported on either decaying amplitude distributions or distributions with a central peak.

Mathematical and computational models offer another angle to help settle these issues. Such models are directly based on the microscopic kinetics of clustered channels. The small number of calcium release channels in a cluster indicates that deterministic models might be insufficient. Thus, there is an increasing interest for the theoretical discussion on the stochastic dynamics of local Ca^{2+} release (Keizer et al., 1998; Swillens et al., 1999; Dawson et al., 1999; Moraru et al., 1999; Falcke et al., 2000; Bar et al., 2000). However, most of these studies focus on the onset of saltatory propagation of Ca^{2+} waves due to intercluster diffusion of Ca^{2+} (Keizer et al., 1998; Falcke et al., 2000). The stochastic dynamics of clustered IP_3Rs has been studied by Swillens et al. (1999) where the IP_3 receptors are assumed to be spatially distributed and coupled by calcium diffusion. The model requires 17 variables for each IP_3 receptor. They suggested that a typical cluster contained 20–30 channels in close contact to ensure efficient interchannel communication.

In this paper we expand the much simpler two-variable Li-Rinzel model (Li and Rinzel, 1994) to its Markov-stochastic version to simulate stochastic calcium release from small clusters of IP_3Rs. In the model, the channels are assumed to be close enough so that Ca^{2+} concentration can be considered homogeneous throughout the cluster. We neglect Ca^{2+} diffusion between cluster and environment without accounting for spatial aspects of the formation and collapse of localized Ca^{2+} elevations. The amplitude, lifetime, and interpuff interval distribution of calcium puffs are discussed. We show that different numbers of IP_3Rs and different IP_3 stimuli can lead to a variety of different amplitude distributions, including simply decaying distributions and single- and double-peaked distributions. Based on the open channel number distributions we infer—consistent with other independent estimates (Swillens et al., 1999)—that the number of channels per cluster is around 20. We also approximate the Markov Li-Rinzel model by a Langevin-type model. It is shown that the Langevin approach is a simple but efficient approximation for the Markov process, even for a cluster with tens of IP_3Rs.

THEORETICAL METHODS

Deterministic Li-Rinzel model

The first theoretical model for agonist-induced $[Ca^{2+}]$ oscillations based on microscopic kinetics of IP_3 and $[Ca^{2+}]$ gating of the IP_3R was proposed by De Young and Keizer (1992). The model assumes that three equivalent and independent subunits are involved in conduction in an IP_3R. Each subunit has one IP_3 binding site and two Ca^{2+} binding sites, one for activation, the other for inhibition. Thus, each subunit may exist in eight states with transitions governed by second-order and first-order rate constants. Only the state with one IP_3 and one activating Ca^{2+} bound contributes to the subunit's open probability. All three subunits must be in this state for the channel to be open. Although the model is unique in giving detailed gating kinetics, the number of variables is relatively high. It involves eight variables plus the concentration of IP_3 as a control parameter. A simplified version of the model was proposed by Li and Rinzel (1994). It is shown that the full De Young-Keizer model is symmetric in some of the binding processes and that the IP_3 binding is at least 200 times faster than the Ca^{2+} activation binding, while the Ca^{2+} activation binding is at least 10 times faster than the Ca^{2+} inactivation binding and the change rate of $[Ca^{2+}]$ during oscillations (Li and Rinzel, 1994). Considering these factors, the De Young-Keizer model can be reduced to the following system of two ordinary differential equations

$$\frac{d[Ca^{2+}]}{dt} = -J_{Channel} - J_{Pump} - J_{Leak} \tag{1}$$

$$\frac{dh}{dt} = \alpha_h(1 - h) - \beta_h h. \tag{2}$$

with $J_{Channel}$ being calcium flux from the ER to the intracellular space through the IP_3R channel, J_{Pump} being the calcium flux pumped from the intracellular space into the ER, and J_{Leak} being leakage flux from the ER to the intracellular space. The expressions for the fluxes are given by

$$J_{Channel} = c_1 v_1 m_\infty^3 n_\infty^3 h^3([Ca^{2+}] - [Ca^{2+}]_{ER}) \tag{3}$$

$$J_{Pump} = \frac{v_3[Ca^{2+}]^2}{k_3^2 + [Ca^{2+}]^2} \tag{4}$$

$$J_{Leak} = c_1 v_2([Ca^{2+}] - [Ca^{2+}]_{ER}) \tag{5}$$

with

$$m_\infty = \frac{[IP_3]}{[IP_3] + d_1}$$

$$n_\infty = \frac{[Ca^{2+}]}{[Ca^{2+}] + d_5}$$

$$\alpha_h = a_2 d_2 \frac{[IP_3] + d_1}{[IP_3] + d_3}$$

$$\beta_h = a_2[Ca^{2+}] \tag{6}$$

The parameters of the model are $c_1 = 0.185$, $v_1 = 6\ s^{-1}$, $v_2 = 0.11\ s^{-1}$, $v_3 = 0.9\ \mu M\ s^{-1}$, $k_3 = 0.1\ \mu M$, $d_1 = 0.13\ \mu M$, $d_2 = 1.049\ \mu M$, $d_3 = 0.9434\ \mu M$, $d_5 = 0.08234\ \mu M$, and $a_2 = 0.2\ \mu M^{-1}\ s^{-1}$. Conservation of

Ca^{2+} implies the constraint $[Ca^{2+}]_{ER} = (c_0 - [Ca^{2+}])/c_1$, with $c_0 = 2.0$ μM. The concentration $[IP_3]$ is a control parameter.

This simplified model resembles the Hodgkin-Huxley (HH) model for electrically excitable membranes if $[Ca^{2+}]$ is replaced by the transmembrane potential. The driving force for Ca^{2+} fluxes is the concentration gradient ($[Ca^{2+}] - [Ca^{2+}]_{ER}$), while the driving force for the ionic currents in the HH equation is the voltage gradient.

Markov-stochastic Li-Rinzel model

Equations 1 and 2 describe the deterministic behavior averaged for a large number of channels. The small number of IP_3Rs in single clusters suggests that a stochastic formulation of these equations is necessary if calcium release from a single cluster is considered. Following the deterministic Li-Rinzel model, we only consider the stochastic opening and closing process for gate h here. Each gate h is an inactivation binding site for Ca^{2+} that is occupied (closing) or non-occupied (open). We describe the binding and unbinding of these three sites by independent two-state Markov processes with opening and closing rates α_h and β_h, respectively.

Thus, instead of Eq. 2, the stochastic scheme for all three gates is postulated

$$C \underset{\beta_h}{\overset{\alpha_h}{\rightleftharpoons}} O \tag{7}$$

Equation 6 shows that the open rate α_h is only determined by $[IP_3]$ and the closing rate β_h is determined by $[Ca^{2+}]$. A single cluster consists of N IP_3Rs with three stochastic h gates each. They are globally coupled by a common but varying $[Ca^{2+}]$.

There are several ways to simulate this stochastic scheme. A widely applied approach is simply to account for the number of channels in each state of the kinetic model (Strassberg and DeFelice, 1993). The IP_3R channel can exist in four different states, and the kinetic scheme describing the behavior of this channel is given by

$$[n_0] \underset{\beta_h}{\overset{3\alpha_h}{\rightleftharpoons}} [n_1] \underset{2\beta_h}{\overset{2\alpha_h}{\rightleftharpoons}} [n_2] \underset{3\beta_h}{\overset{\alpha_h}{\rightleftharpoons}} [n_3] \tag{8}$$

where $[n_i]$ is the number of the channels with i open gates, and hence $[n_3]$ labels the open state of the IP_3R channel. The total population of channels in each of their possible states will be tracked with time.

One can also directly simulate the stochastic dynamics of Eq. 7 for each single gate by a two-state Markov process (Jung and Shuai, 2001). This scheme can be expressed directly in terms of a computer algorithm. In detail, the state of the system is updated for every small time step δt. Each IP_3R channel has three two-state h gates. If an h gate is closed at time t, then the probability that it remains closed at time $t + \delta t$ is $\exp(-\alpha_h \cdot \delta t)$, and if it is open at time t, then the probability that it remains open at time $t + \delta t$ is $\exp(-\beta_h \cdot \delta t)$. To determine the state of a gate, random numbers are drawn consistent with these probabilities. Only if all three h gates in an IP_3R channel are open at time t, which means there is no Ca^{2+} bound at each of the three inactivation Ca^{2+} sites, the channel is h disinactivated or h-open. The probability that a h-open channel is conducting Ca^{2+} is given by $m_\infty^3 n_\infty^3$. The expression for the calcium flux through the IP_3R channels replacing Eq. 3 is given by

$$J_{Channel} = c_1 v_1 m_\infty^3 n_\infty^3 \frac{N_{h-open}}{N} ([Ca^{2+}] - [Ca^{2+}]_{ER}) \tag{9}$$

where N and $N_{h\text{-}open}$ indicate the total number of IP_3R channels and the number of h-open channels, respectively. $N_{h\text{-}open}/N$ is the h-open fraction, replacing h^3 in Eq. 3 of the deterministic model. Note that the h-open fraction in this method becomes a discrete variable with only $N + 1$ possible values, rather than a continuous variable.

In this paper we discuss the Markov dynamics of calcium release events for different IP_3R numbers N and stimuli $[IP_3]$. Note that the maximum flux rate $c_1 v_1$ of the IP_3R channels is constant for varying N in our simulation. In experiments, $[IP_3]$ can be stimulated and adjusted by the binding of an extracellular agonist such as a hormone or a neurotransmitter to receptors in the surface membrane (Callamaras et al., 1998; Sun et al., 1998).

In the model, we did not account for spatial aspects of the formation and collapse of localized Ca^{2+} elevations. The role of Ca^{2+} diffusion between the cluster and the environment in the dynamics of Ca^{2+} puff formation is neglected. However, the channels are assumed to be close enough so that the Ca^{2+} concentration within a cluster is homogeneous due to instantaneous Ca^{2+} diffusion (Swillens et al., 1999). In experiment, to study the dynamics of puffs or sparks, the clusters have to be functionally isolated. This is the case if the IP_3 concentration is low (Sun et al., 1998) and the calcium diffusion coefficient is small (Callamaras and Parker, 2000). Experimentally, weak Ca^{2+} diffusion can be achieved by intracellularly loading with the Ca^{2+} buffer EGTA (Mak and Foskett, 1997; Horne and Meyer, 1997; Thomas et al., 1998; Marchant et al., 1999; Cheng et al., 1999; Callamaras and Parker, 2000; Rios et al., 2001). With a large loading of EGTA, the clusters become functionally isolated even at large concentrations of IP_3 (Horne and Meyer, 1997; Thomas et al., 1998; Callamaras and Parker, 2000). Short-range feedback (within 0.2 μm) between individual IP_3Rs in one cluster is still intact. Thus, even with a larger IP_3 concentration, single release sites can be studied. For this experimental design our separated-cluster model with homogeneous calcium is applicable.

Langevin approach

The Markov method is conceptually simple and very accurate, as long as the random number generator is adequate and the time step δt is small compared with the speed of fluctuations of the Ca^{2+} signal and channel state. However, this method is inefficient, especially for a large number of channels. It requires a large array to store the state of each gate and the generation of $3N$ random numbers for each time step. In the following we discuss under what conditions the Markov approach can be approximated by a Fokker-Planck equation, or equivalently by a Langevin equation for the fraction of open inactivation gates.

Because the time scale for $[Ca^{2+}]$ in the dynamic equations is the slowest, we consider the gate dynamics with constant $[Ca^{2+}]$ during each time step of iteration (0.01 s). For each gate ($i = 1, 2, 3$) we can write down a master equation for the numbers n_i of IP_3Rs with open gate i (Fox and Lu, 1994)

$$\begin{aligned}\dot{P}(n_i, t) = {} & (N - n_i + 1)\alpha_h P(n_i - 1, t) \\ & + (n_i + 1)\beta_h P(n_i + 1, t) \\ & - (n_i\beta_h + (N - n_i)\alpha_h)\, P(n_i, t)\end{aligned} \tag{10}$$

For a large number N, this master equation can be approximated by a Fokker-Planck equation, which is a linear partial differential equation for the probability of fraction of h-open gates $h_i = n_i/N$ (Van Kampen, 1976). For every Fokker-Planck equation there is a statistically equivalent set of Langevin equations, i.e., a set of stochastic differential equations (Fox and Lu, 1994). The Langevin equation for the fraction of h-open gate $h_i = n_i/N$ is then expressed as (Fox and Lu, 1994; Fox, 1997)

$$\frac{dh_i}{dt} = \alpha_h(1 - h_i) - \beta_h h_i + G_{h_i}(t) \tag{11}$$

where $G_{h_i}(t)$ are zero mean, uncorrelated, Gaussian white-noise terms with

$$\langle G_{h_i}(t)G_{h_j}(t')\rangle = \frac{\alpha_h(1-h_i)+\beta_h h_i}{N}\,\delta(t-t')\delta_{ij}, \quad (12)$$

and $i, j = 1, 2, 3$. The Langevin approach indicates that the stochastic dynamics of the IP_3R cluster can be treated as a deterministic dynamics disturbed by a Gaussian white noise.

The stochastic equation for $[Ca^{2+}]$ flux through the IP_3R is given by

$$J_{\text{Channel}} = c_1 v_1 m_\infty^3 n_\infty^3 h_1 h_2 h_3([Ca^{2+}] - [Ca^{2+}]_{ER}) \quad (13)$$

which replaces the $[Ca^{2+}]$ flux through the IP_3R in Eq. 3. To further simplify the problem we replace $h_1h_2h_3$ by h^3, where h obeys Eq. 11. Thus, instead of applying independent fluctuation for each h gate of IP_3R, three identical h gates are assumed. The gain in computational speed is a factor of three. The error calculated from the mean values of $[Ca^{2+}]$, $\langle[Ca^{2+}]\rangle$ through this approximation is $<5\%$ for $N = 15$ and $<0.5\%$ for $N = 1000$ and various $[IP_3]$ (a comparison of $\langle[Ca^{2+}]\rangle$ between these two approaches is given in Fig. 5 for $N = 20$, which is a realistic size of a cluster (Swillens et al., 1999)).

In the simulation, the Gaussian noise sources are generated at each integration step by the Box-Muller algorithm. Since h has to be bound between 0 and 1, it is necessary to verify this condition after each iteration step. The approximate nature of Eq. 11 does not automatically maintain h_i in the required interval. We simply disregard an iteration step that leads to a negative value for h. Simulation shows that the results are insensitive to the choice of strategy to keep h in [0,1].

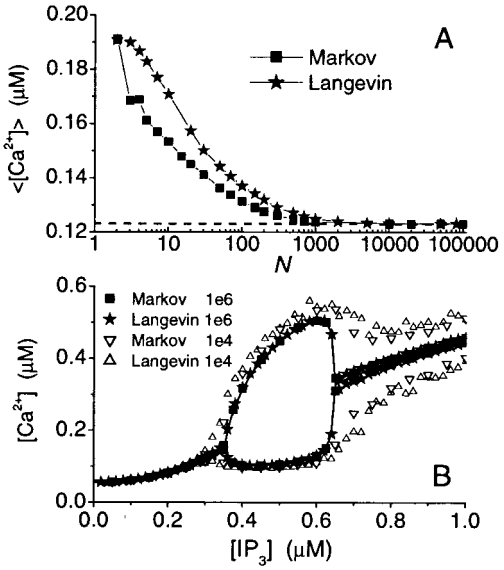

FIGURE 1 (*A*) Both stochastic models approach the deterministic Li-Rinzel model at large N. In (*a*) we show the mean value of Ca^{2+} versus N obtained with the Markov method (*solid square*) and the Langevin approach (*solid star*). The deterministic limit of $[Ca^{2+}]$ is also shown by a dotted line. In (*B*) the bifurcation diagram of the stochastic Li-Rinzel model, obtained with Markov and Langevin methods, is compared with the deterministic result (*solid line*).

RESULTS

Approaching a deterministic model with large *N*

The C++ language is used for programming. We simulate the stochastic equations by using an explicit first-order algorithm with a time step of 0.01 s, smaller than the time constant of the h gate, e.g., $\tau_h = 1/(\alpha_h + \beta_h) > 3$ s for $[Ca^{2+}] < 1.0\ \mu$M and $[IP_3] < 1.0\ \mu$M. Consistent results are obtained by changing the time step and the total simulation time.

In Fig. 1 we demonstrate that for large numbers of channels, both stochastic methods reproduce the features of the deterministic Li-Rinzel model. As $[IP_3] = 0.3\ \mu$M (Fig. 1 *A*), the average Ca^{2+} concentration approaches the deterministic limit (*dashed line*) at large N. In Fig. 1 *B* we show that the entire bifurcation diagram is being reproduced by the stochastic model at large N. While the deterministic Li-Rinzel model predicts oscillation for $0.354\ \mu\text{M} < [IP_3] < 0.642\ \mu$M (minima and maxima plotted), it predicts fixed points anywhere else. For $N = 10^6$, this bifurcation diagram is well-reproduced by both stochastic methods (Fig. 1 *B*). This argument is obvious since Eq. 11 approaches Eq. 2 for $N \to \infty$, and the Langevin equation is the leading order approach to the exact Markov equation (Eq. 10) as the size of the fluctuations is expanded in order of $1/N$. The main advantage of the Langevin approach is that the computing times do not depend on the number of channels, as they do with the Markov method.

Stochastic oscillation

It is suggested that IP_3R clusters typically contain several or tens of IP_3R channels (Mak and Foskett, 1997; Bootman et al., 1997; Sun et al., 1998; Swillens et al., 1999). In the following we limit our discussion to $N \leq 100$. In our simulations, different $[IP_3]$ stimuli (i.e., $[IP_3] = 0.3$, 0.5, and $0.8\ \mu$M) are selected to represent the three deterministically distinguished regions (fixed point, oscillation, fixed point).

In Fig. 2 *A* we show results obtained with the Markov method for $N = 20$ and three values of $[IP_3]$. For $[IP_3] = 0.3\ \mu$M, the deterministic dynamics gives a stable fixed point. The stochastic openings of h gates, however, initiate stochastic Ca^{2+} release, i.e., puffs. The elevated values of $[Ca^{2+}]$ in turn lead to large h-gate closing rates and termination of puffs. For $[IP_3] = 0.3\ \mu$M, we have $m_\infty = 0.7$ and $\alpha_h = 0.07$. If $[Ca^{2+}]$ increases from 0.1 to 0.5 μM, m_∞ increases by 67% from 0.55 to 0.86, while β_h increases by 400% from 0.02 to 0.1. This large increase of Ca^{2+}-dependent inhibition (β_h) causes the termination of puffs. For $[IP_3] = 0.8\ \mu$M, the deterministic model gives a spiral fixed point with a pair of complex conjugate eigenvalues. For small IP_3R clusters, fluctuations will initiate large lightly damped stochastic oscillations. As a result, the Ca^{2+} trajectory spends less time at the stable fixed point than that of $[IP_3] = 0.3\ \mu$M (Fig. 2 *A*). However, as N gets larger fluctuations become smaller, and so the stochastic Ca^{2+} oscillation will be closer to the fixed point.

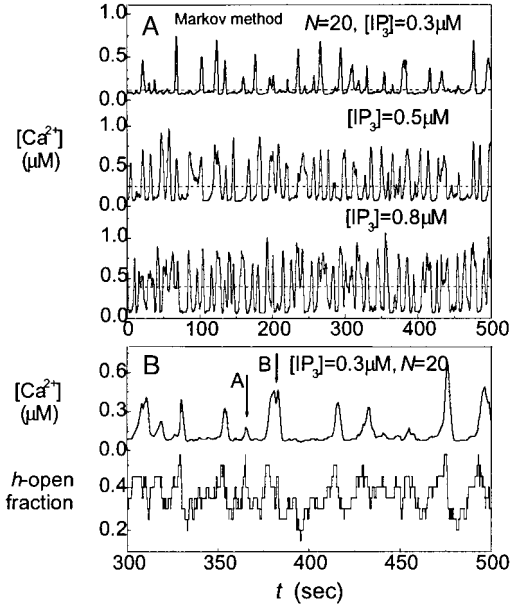

FIGURE 2 (*A*) Stochastic oscillation of the calcium release of a cluster of 20 IP_3Rs obtained with the Markov method at $[IP_3] = 0.3$, 0.5, and 0.8 μM. The dotted line is for the result obtained with the deterministic model. (*B*) A calcium trace is compared with the associated trace of the fraction of *h*-open channels for $N = 20$ and $[IP_3] = 0.3$ μM.

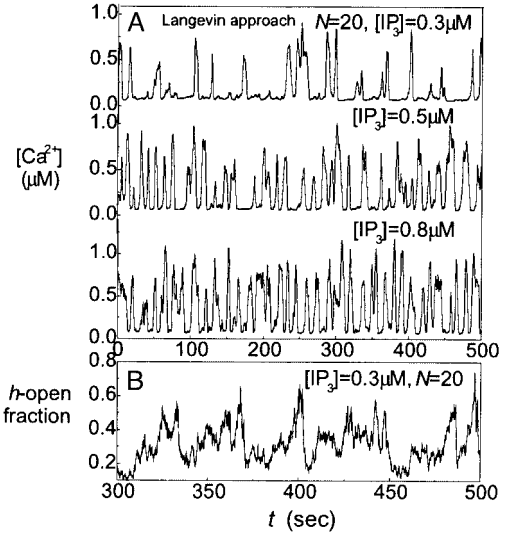

FIGURE 3 (*A*) Stochastic oscillation of the calcium release of a cluster of 20 IP_3Rs with the Langevin approach is shown for $[IP_3] = 0.3$, 0.5, and 0.8 μM. (*B*) The trace of the fraction of *h*-open channels for $N = 20$ and $[IP_3] = 0.3$ μM.

Most notably, the Ca^{2+} trace in the deterministically oscillatory regime can hardly be distinguished from the other traces with respect to periodicity. They are strongly dominated by the stochastic opening and closing of IP_3Rs. Thus, it is evident that the Ca^{2+} release from clusters of sizes that are believed realistic cannot be described by a deterministic equation. The Ca^{2+} signal trace appears as stochastic in the deterministically oscillating regime as it appears in the deterministically non-oscillating regimes.

The amplitudes and durations of release events (puffs) are determined by the fractions of *h*-open channels and their opening durations. The importance of the opening duration is substantiated in Fig. 2 *B*. The calcium amplitude of puff A is smaller than that of puff B, but the corresponding *h*-open fraction of puff A is larger than that of puff B.

In Fig. 3 *A* we show the Ca^{2+} signals obtained with the Langevin approach for $N = 20$. A plot of *h*-open fraction $h(t)$ is shown in Fig. 3 *B* for $[IP_3] = 0.30$ μM and $N = 20$. Comparing Figs. 2 *B* and 3 *B* it can be seen that the Langevin method gives a slightly larger probability for large or small *h*.

Mean value and variance of $[Ca^{2+}]$

In this section we compare statistical properties of the calcium release using the Markov method and the Langevin approach. In Fig. 4 *A* the mean value $\langle[Ca^{2+}]\rangle$ is plotted as a function of the cluster size. The Langevin approach yields results that agree qualitatively with Markov simulations even for a few tens of IP_3Rs. Simulations show that for $N = 20$, which is a realistic size of a cluster (Swillens et al., 1999), the results for $\langle[Ca^{2+}]\rangle$ agree within 10% error (Fig. 5); for $N = 15$, the results agree within 12% error with various $[IP_3]$.

It is interesting to note that $\langle[Ca^{2+}]\rangle$ decreases with increasing cluster size for $[IP_3] = 0.3$ or 0.5 μM, while it increases for $[IP_3] = 0.8$ μM, as shown in Fig. 4 *A*. At small values of $[IP_3]$, the baseline of $[Ca^{2+}]$ is close to the deterministically predicted value, and very small. Thus,

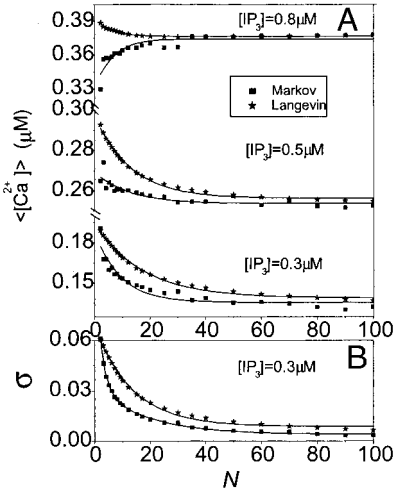

FIGURE 4 Time average of the calcium signal as a function of the cluster size N at $[IP_3] = 0.30$, 0.50, and 0.8 μM (*A*). Variance of the calcium signal as a function of the cluster size N at $[IP_3] = 0.30$ μM (*B*). The results obtained with the Markov method and with the Langevin approach are marked by solid squares and stars, respectively.

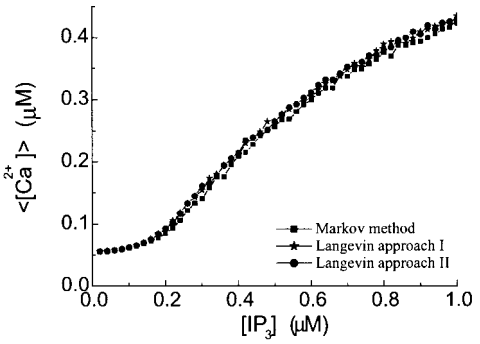

FIGURE 5 Average of the calcium signal as a function of $[IP_3]$ for $N = 20$. The square indicates results obtained with the Markov method. The star represents results obtained with the single Langevin equation for three identical h gates. The circle represents results obtained with three Langevin equations for three different h gates.

fluctuations of the fraction of channel openings mainly yield the increase of $[Ca^{2+}]$ (see Fig. 2 *A*), resulting in the increase of $\langle[Ca^{2+}]\rangle$ in comparison to the deterministic value. With large $[IP_3]$ (e.g., 0.8 μM), the stochastic channel closings, to the contrary, can lead to a large decrease of $[Ca^{2+}]$, compared to $[Ca^{2+}]$ in the deterministic case (see Fig. 2 *A*). Fig. 4 *A* also shows that the Langevin approach gives a wrong prediction for $[IP_3] = 0.8$ μM with small N.

In Fig. 4 *B* the time averaged variance $\sigma = \langle([Ca^{2+}] - \langle[Ca^{2+}]\rangle)^2\rangle$ is shown as a function of the cluster size N for $[IP_3] = 0.3$ μM. Similar results are obtained for $[IP_3] = 0.5$ and 0.8 μM (not shown). The variance decreases with increasing cluster size, which is also predicted by the Langevin approach with Eq. 12. In the oscillatory regime, the variance does not approach zero as $N \to \infty$, the same as the deterministic limit.

Amplitude distribution of puffs

Fig. 2 *B* shows that the number of IP_3Rs recruited in the Ca^{2+} puffs varies from puff to puff. Thus, the amplitudes and durations of the Ca^{2+} puffs vary. Important, and experimentally recorded, characteristics of these variabilities are amplitude, lifetime, and interpuff-interval distributions (Pratusevich and Balke, 1996; Bootman et al., 1997; Smith et al., 1998; Izu et al., 1998; Sun et al., 1998; Thomas et al., 1998; Cheng et al., 1999; Jiang et al., 1999; Callamaras and Parker, 2000; Marchant and Parker, 2001; Rios et al., 2001). For the analysis of these distributions of puffs, we apply a cutoff filter at a $[Ca^{2+}]$ of 0.2 μM to mimic a noise floor.

The shape of the puff amplitude distribution depends on the concentration of $[IP_3]$ and the size of the cluster, characterized by the number of IP_3Rs in the cluster. An approximate *phase diagram* is shown in Fig. 6 *A* for $N \leq 100$ and $[IP_3] \leq 1.0$ μM obtained with the Markov method. If the $[IP_3]$ stimulus is quite small, the amplitudes of the spontaneous puffs are typically smaller than 0.2 μM and are

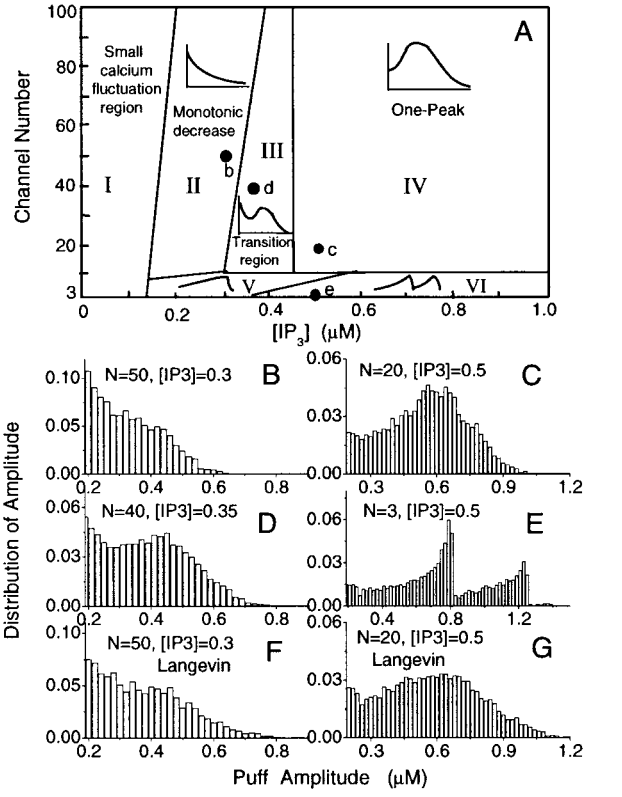

FIGURE 6 Phase diagram of the puff amplitude distributions is shown in (*A*) in the $[IP_3]$-N-plane. Samples of puff amplitude distributions obtained with the Markov method are shown in (*B*)–(*E*) in various regimes indicated in (*A*). Panels (*F*) and (*G*) show the amplitude distribution obtained with the Langevin approach in comparison to those obtained with the Markov method in (*B*) and (*C*).

regarded as noise floor. For clusters with tens of IP_3Rs, monotonically decreasing amplitude distributions are mainly found for small $[IP_3]$ stimulus (region II in Fig. 6 *A*). Single-peak amplitude distributions are mainly found for large $[IP_3]$ (region IV in Fig. 6 *A*). In Fig. 6, *B* and *C* we show characteristic amplitude distributions in regions II and IV. The transition from regions II to IV is continuous in that a peak that eventually dominates for large enough $[IP_3]$ develops additional to the decay at small amplitudes (region III in Fig. 6 *A*, or see Fig. 6 *D*).

For clusters with only a few IP_3Rs, single-peak amplitude distributions are observed in region V of Fig. 6 *A*; two-peak distributions are observed in region VI (see Fig. 6 *E*). Different from the single-peak puff amplitude distributions in region IV, the single-peak distribution for a few IP_3Rs in region V is strongly asymmetric, with a slow increase and a rapid fall-off.

The amplitude distributions obtained from the Langevin approach are also compared with the Markov method. It is shown that when N is $>\sim 15$, both distributions exhibit similar shapes. As two examples, one can compare Fig. 6, *B* and *f* for $N = 50$, or Fig. 6, *C* and *G* for $N = 20$. It is also

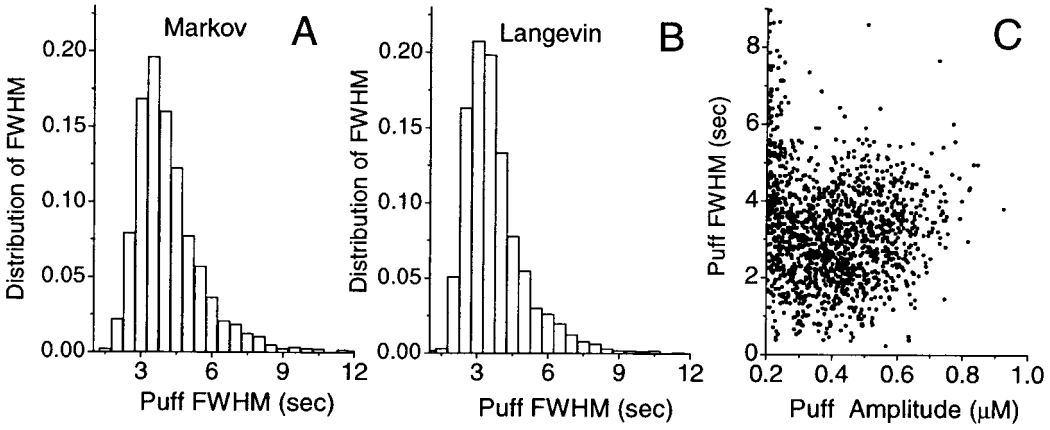

FIGURE 7 Lifetime distributions of puffs obtained with the Markov method (*A*) and the Langevin approach (*B*) are shown at $N = 20$ and $[IP_3] = 0.3$ μM. The amplitude-lifetime scatter plot (*C*) demonstrates small correlations between lifetime and amplitudes of puffs.

shown that the Langevin approach yields more puffs with larger amplitudes, which leads to (via the normalization) a drop-off of distribution at smaller amplitude.

Fig. 6 *A* shows that different distributions of puff amplitudes can be observed at different $[IP_3]$ and N. The particular value of N does not influence the different phases very much for $10 < N < 100$. The phase boundaries are mostly determined by $[IP_3]$. For $N > 10$, the Markov process can be approached by the Langevin approach, suggesting that the stochastic cluster-dynamics can be considered as a deterministic dynamics perturbed by Gaussian noise. In region II (see Fig. 6 *A*), where the deterministic dynamics approaches a small fixed point, we thus expect a simply decaying distribution of puff amplitude. For increasing $[IP_3]$, the Hopf-bifurcation in the deterministic equation introduces an oscillatory component of the calcium dynamics, giving rise to a characteristic amplitude, manifesting in the peak of the puff amplitude distribution in III and the part of IV with $[IP_3] < 0.64$ μM. For $[IP_3] > 0.64$ μM, the deterministic dynamics predicts a large stationary $[Ca^{2+}]$. Channel noise gives rise to a distribution of puff amplitude around this value.

The shapes of the puff amplitude distributions are consistent with observed amplitude distributions in experiments from *Xenopus* oocytes and HeLa cells (Sun et al., 1998; Thomas et al., 1998; Marchant and Parker, 2001; Haak et al., 2001).

Lifetime distribution of puffs

In addition to a wide distribution of Ca^{2+} puff amplitudes, considerable variations of lifetimes have been observed experimentally (Sun et al., 1998; Thomas et al., 1998; Haak et al., 2001). The lifetimes of puffs are measured as their full width at half-maximal amplitude (FWHM). In other words, FWHM is defined here as the time interval for which the calcium concentration profile is above one-half of the maximum concentration reached during the puff. Because the model presented does not include a spatial aspect, it is impossible to compare to FWHM in the sense of puff width (as done by Smith et al. (1998)).

Compared to various types of amplitude distribution, numerical simulation shows that the shapes of the FWHM distribution turn out to be more uniform. A typical FWHM distribution is shown in Fig. 7 *A* for $[IP_3] = 0.3$ μM and $N = 20$. It exhibits a single peak at $\sim$3 s, i.e., most frequently, the duration of a puff is $\sim$3 s. For $N < 10$ and $IP_3 \geq 0.6$ μM, a monotonically decreasing distribution is found with the Markov method. The Langevin approach can reproduce the lifetime distribution of puffs satisfactorily (see Fig. 7 *B*).

A broad distribution of lifetimes is also observed in experiments for HeLa or oocyte cells (Sun et al., 1998; Thomas et al., 1998). A difference is that the characteristic time scale of calcium puff for HeLa or oocyte cells is $\sim$100 ms, but the characteristic time scale for the Li-Rinzel model is $\sim$1 s. The time scale for oscillations in the Li-Rinzel model is related to the rate of the IP_3R inactivation process. If a proper inactivation rate is set in the model, shorter lifetimes can then be observed. However, it is also possible that in HeLa and oocyte cells the buffered diffusion of intracellular Ca^{2+} can affect the lifetime of puffs, which is not addressed in the current model.

Correlation between amplitude and lifetime of puffs

Experimental observations indicate small correlations between puff amplitudes and durations (Thomas et al., 1998). Fig. 7 *C* shows a scatter plot of puff amplitudes versus lifetimes at $[IP_3] = 0.3$ μM and $N = 20$. Similar plots are obtained for different values of $[IP_3]$ and N. A large puff amplitude does not correlate with a large lifetime, and vice versa (also see Fig. 2 *B*). Therefore, one can observe a puff

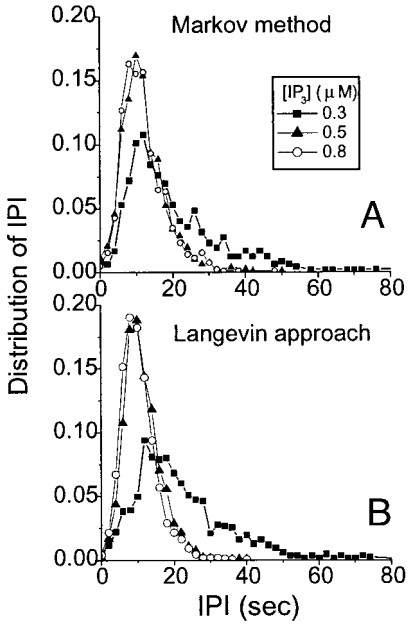

FIGURE 8 Interpuff-interval distributions of puffs obtained with the Markov method (*A*) and the Langevin approach (*B*) are shown at $N = 20$ and $[IP_3] = 0.3$ μM (*solid square*), 0.5 μM (*solid triangle*), and 0.8 μM (*open circle*).

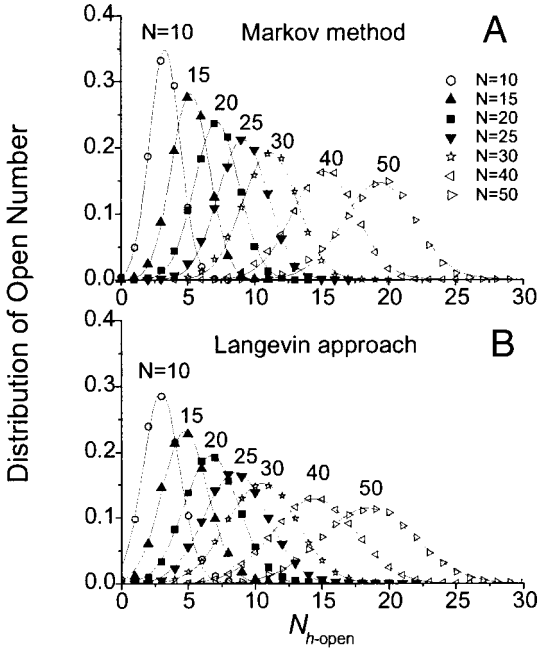

FIGURE 9 Distribution of *h*-open channel numbers for $[IP_3] = 0.3$ μM and various cluster sizes $N = 10$, 15, 20, 25, 30, 40, and 50 with the Markov method (*A*) and the Langevin approach (*B*). For $N = 20$, e.g., the most likely number of recruited channels of a puff is 7.

with a large amplitude but short duration, or a puff with a small amplitude but long duration.

To quantitatively discuss the correlation between puff amplitude x_1 and lifetime x_2 of puffs, the correlation ξ is calculated with the following equation:

$$\xi = \frac{\langle (x_1 - \langle x_1 \rangle)(x_2 - \langle x_2 \rangle) \rangle}{(\langle (x_1 - \langle x_1 \rangle)^2 \rangle)^{1/2} (\langle (x_2 - \langle x_2 \rangle)^2 \rangle)^{1/2}} \qquad (14)$$

Simulation results show that the correlation values are typically smaller than 0.3 for various N and $[IP_3]$.

Interpuff-interval distribution of puffs

Another important characteristics of calcium puffs is the distribution of times between two consecutive puffs. Recent experimental investigation (Marchant et al., 1999) has revealed interpuff-interval (IPI) distribution that exhibits a single peak mode. The IPIs obtained with the Markov method and Langevin approach for $[IP_3] = 0.3$, 0.5, and 0.8 μM are shown at $N = 20$ in Fig. 8, *A* and *B*, respectively. The IPIs resulting from the Langevin approach agree with those obtained with the Markov method (Fig. 8, *A* and *B*), although the lifetime distributions of puffs are not well described by the Langevin method (Fig. 7, *A* and *B*).

Size of IP_3R clusters

An important question is the number of IP_3Rs in a cluster. Experiments with *Xenopus* oocytes suggest that approximately five to eight spontaneously open IP_3Rs can be observed in a cluster (Mak and Foskett, 1997; Sun et al., 1998). Fig. 9 *A* shows the distributions of *h*-open IP_3Rs obtained from the Markov method for various cluster sizes N at $[IP_3] = 0.3$ μM. This value is motivated by experiments that need this $[IP_3]$ to stimulate puffs. For the Langevin approach, the *h*-open fraction (i.e., h^3) is a continuous number between 0 and 1. The corresponding distribution of $N_{\text{h-open}} \equiv (\text{integer})(h^3 N)$ is shown in Fig. 9 *B* at $[IP_3] = 0.3$ μM for various N. It can be seen that both methods yield consistent distributions.

Fig. 9 indicates that the larger the cluster, the more unlikely is the opening of a small number of IP_3Rs. Thus, given the typical number of five to eight spontaneously open IP_3Rs, we can conclude from Fig. 9 that the sizes of the clusters are $\sim 15-25$ IP_3Rs. This result is consistent with the theoretical estimate of the cluster size by Swillens et al. (1999). They predict 20–30 IP_3Rs per cluster based on the requirement of interchannel communication.

DISCUSSION AND SUMMARY

Previous work showed that IP_3-mediated global Ca^{2+} signals can be devolved into localized Ca^{2+} release events due to the clustered distribution of IP_3Rs (Bootman et al., 1997). Furthermore, observations of signals of differing magnitudes suggested a hierarchy of calcium signaling events from small blips to large puffs (Lipp and Niggli, 1998;

Bootman et al., 1997). Improved spatial and temporal resolution in recording reveal that there is not a clear distinction between fundamental blips and elementary puffs. A continuum of Ca^{2+} release signals can be achieved due to stochastic variation in both numbers of channels recruited and durations of channel openings within a cluster (Bootman et al., 1997; Sun et al., 1998; Thomas et al., 1998; Callamaras and Parker, 2000; Marchant and Parker, 2001; Haak et al., 2001).

We have put forward a Markov version of the Li-Rinzel (1994) model to study the statistical properties of Ca^{2+} release of clusters of IP_3Rs. In comparison to the other Markov IP_3R channel models (Falcke et al., 2000; Bar et al., 2000; Swillens et al., 1999), our model is relatively simple and is represented by only two variables in the deterministic limit.

The small size of the IP_3Rs introduce stochastic oscillation into the calcium release dynamics. The stochastic oscillations are different from the stochastic excitability discussed by Keizer and Smith (1998). For the stochastic excitability, once $[Ca^{2+}]$ randomly becomes larger than a threshold, a fast release (action-potential-like) of $[Ca^{2+}]$ followed by a refractory period can be observed. For the stochastic oscillation there is not such a threshold. More broad distributions of puff amplitudes and lifetime are yielded for stochastic oscillation.

Calcium puffs vary in amplitude, lifetime, and interpuff-interval (Figs. 5–7) due to the variability of numbers of recruited channels and their open duration. This result indicates that a fixed puff morphology (i.e., amplitude and lifetime), which is sometimes assumed in literature (Pratusevich and Balke, 1996; Izu et al., 1998; Cheng et al., 1999) is not a good assumption for Ca^{2+} puff analysis.

The shape of puff amplitude distribution was a subject of a recent controversy. Although in experiment single-peak amplitude distributions are typically observed, theoretical study indicated that this feature could be caused by the failure of detecting small-amplitude puffs due to the confocal response function. Cheng et al. (1999) suggested that the original calcium puffs should exhibit an exponentially decaying amplitude distribution, regardless of whether the underlying events are stereotyped. Recently, however, Rios et al. (2001) presented new data with either decaying amplitude distributions or single-peak amplitude distributions. They suggested that if sparks were produced by individual Markovian release channels evolving reversibly, the amplitude distribution should be simply decaying. Channel groups typically give rise to a peak mode distribution in their collective spark.

Our Markov model suggests that both types of puff amplitude distributions are possible, depending on the size of the cluster and the level of $[IP_3]$. For tens of channels and small $[IP_3]$ the puff amplitude distributions are typically simply decaying due to the small mean value of Ca^{2+} signals, while for a large $[IP_3]$ the stochastic dynamics leads a single peak amplitude distribution around the large mean value.

The amplitude and duration of puffs are related to the fraction and duration of open IP_3Rs in a cluster. Roughly, a large-amplitude puff correlates with a large fraction of *h*-open IP_3Rs, and a long lifetime of puffs correlates with a long duration of an *h*-open fraction. However, a large puff may also be caused by a small fraction of IP_3Rs, but with a long duration. To typically observe five to eight spontaneously open channels, we estimate based on the Markov Li-Rinzel model that a single cluster typically includes 15–25 IP_3Rs. This result is consistent with the estimation obtained with independent methods (Swillens et al., 1999).

To shortcut the computationally expensive Markov simulations of the Ca^{2+} release of a cluster of IP_3Rs, we have introduced a Langevin-type description that is analogous to the one put forward by Fox and Lu (1994) for the Hodgkin-Huxley neuron. It is shown that, even for tens of IP_3Rs, the Langevin approximation can be used as a simple but efficient approach for the Markov process.

In this simple stochastic clustered IP_3R model, spatial aspects of the formation and collapse of localized Ca^{2+} elevations are neglected. The Ca^{2+} diffusion between the cluster and the environment is ignored so that an isolated cluster can be discussed. However, the channels are assumed to be close enough and the instantaneous Ca^{2+} diffusion within a cluster is so fast that the calcium concentration within a cluster is always homogeneous.

To observe puffs or sparks in the experiment, calcium diffusion is suppressed by intracellular loading with the Ca^{2+} buffer EGTA (Mak and Foskett, 1997; Horne and Meyer, 1997; Thomas et al., 1998; Marchant et al., 1999; Cheng et al., 1999; Callamaras and Parker, 2000; Rios et al., 2001). With a large loading of EGTA, the clusters become functionally isolated (Callamaras and Parker, 2000). Under these condition, our model is valid.

Experimental and theoretical work (Roberts, 1993; Bertram et al., 1999) suggests that even at steady state the Ca^{2+} diffusion at a Ca^{2+} release site may lead to inhomogeneous profiles, suggesting that the diffusion within a cluster may affect the puff dynamics. However, a more realistic model put forward by Swillens et al. (1999) shows that the simplification applied in our paper affects the main results only insignificantly. Swillens et al. (1999) considered a stochastic clustered IP_3R model within a 3-D Cartesian space. Each channel occupies a certain position inside the cluster on the ER membrane and is in contact with the Ca^{2+} concentration in the adjacent small cubic volume. Their simulation result suggested that a typical cluster could contain 20–30 channels. Their data also showed that the distribution of puff amplitudes is monotonically decreasing for a small $[IP_3]$ and $N = 25$, and has a single-peak mode for large $[IP_3]$. Based on the discussion of a simplified model, they indicated that the kinetic behavior of a cluster could be satisfactorily simulated by considering a virtual domain in which

all of the channels of a cluster and the calcium concentration were homogeneously distributed.

Three distinct physiological mechanisms have been proposed to underlie Ca^{2+} release and uptake in cells: excitable, oscillatory, and bistable states. All three physiological states can be derived from a Li-Rinzel model with different parameters (Keizer and Smith, 1998). It is interesting to discuss how the stochastic properties of dynamics of Ca^{2+} release depend on the different dynamics states, which is the subject of our current research and will be discussed in a forthcoming paper.

The stochastic oscillation for small $[IP_3]$ facilitates Ca^{2+} signals that may regulate other cell functions. One could hypothesize that the small cluster size serves exactly this purpose. In a recent paper (Shuai and Jung, 2002), this hypothesis is supported by the coherence analysis of Ca^{2+} signals released from a single cluster. The behavior of coherence resonance (Pikovsky and Kurths, 1997) is found for $[IP_3] < 0.354\ \mu M$, suggesting that the regularity of calcium signaling can be optimized at a certain cluster size.

This material is based upon work supported by the National Science Foundation under Grant IBN-0078055. We have greatly benefited from discussions with Martin Falcke from the Hahn-Meitner Institute in Berlin, Germany.

REFERENCES

Allen, G. J., S. P. Chu, K. Schumacher, C. T. Shimazaki, D. Vafeados, A. Kemper, S. D. Hawke, G. Tallman, R. Y. Tsien, J. F. Harper, J. Chory, and J. I. Schroeder. 2000. Alteration of stimulus-specific guard cell calcium oscillations and stomatal closing in Arabidopsis det3 mutant. *Science.* 289:2338–2342.

Bar, M., M. Falcke, H. Levine, and L. S. Tsimring. 2000. Discrete stochastic modeling of calcium channel dynamics. *Phys. Rev. Lett.* 84: 5664–5667.

Bertram, R., G. D. Smith, and A. Sherman. 1999. Modeling study of the effects of overlapping Ca^{2+} microdomains on neurotransmitter release. *Biophys. J.* 76:735–750.

Bezprovanny, I., J. Watras, and B. Ehrlich. 1991. Bell-shaped calcium response curves of Ins(1, 4, 5) P3- and calcium-gated channels from endoplasmic reticulum of cerebellum. *Nature.* 351:751–754.

Bootman, M., E. Niggli, M. Berridge, and P. Lipp. 1997. Imaging the hierarchical Ca^{2+} signaling system in HeLa cells. *J. Physiol.* 499: 307–314.

Callamaras, N., J. S. Marchant, X. Sun, and I. Parker. 1998. Activation and co-ordination of $InsP_3$-mediated elementary Ca^{2+} events during global Ca^{2+} signals in Xenopus oocytes. *J. Physiol.* 509:81–91.

Callamaras, N., and I. Parker. 2000. Phasic characteristic of elementary Ca^{2+} release sites underlies quantal responses to IP_3. *EMBO J.* 19: 3608–3617.

Cheng, H., W. J. Lederer, and M. B. Cannel. 1993. Calcium sparks: elementary events underlying excitation-contraction coupling in heart muscle. *Science.* 262:740–744.

Cheng, H., L. Song, N. Shirokova, A. Gonzalez, E. G. Lakatta, E. Rios, and M. D. Stern. 1999. Amplitude distribution of calcium sparks in confocal images: theory and studies with an automatic detection method. *Biophys. J.* 76:606–617.

Cornell-Bell, A. H., S. M. Finkbeiner, M. S. Cooper, and S. J. Smith. 1990. Glutamate induces calcium waves in cultured astrocytes: long-range glial signaling. *Science.* 247:470–473.

Dawson, S. P., J. Keizer, and J. E. Pearson. 1999. Fire-diffuse-fire model of dynamics of intracellular calcium waves. *Proc. Natl. Acad. Sci. U.S.A.* 96:6060–6063.

De Young, G. W., and J. Keizer. 1992. A single-pool inositol 1,4,5-trisphosphate-receptor-based model for agonist-stimulated oscillations in Ca^{2+} concentration. *Proc. Natl. Acad. Sci. U.S.A.* 89:9895–9899.

Falcke, M., L. Tsimring, and H. Levine. 2000. Stochastic spreading of intracellular Ca^{2+} release. *Phys. Rev. E.* 62:2636–2643.

Fox, R. F. 1997. Stochastic versions of the Hodgkin-Huxley equations. *Biophys. J.* 72:2068–2074.

Fox, R. F., and Y. Lu. 1994. Emergent collective behavior in large numbers of globally coupled independently stochastic ion channels. *Phys. Rev. E.* 49:3421–3431.

Golovina, V. A., and M. P. Blaustein. 1997. Spatially and functionally distinct Ca^{2+} stores in sarcoplasmic and endoplasmic reticulum. *Science.* 275:1643–1648.

Gonzalez, A., W. G. Kirsch, N. Shirokova, G. Pizarro, G. Brum, I. N. Pessah, M. D. Stern, H. Cheng, and E. Rios. 2000. Involvement of multiple intracellular release channels in calcium sparks of skeletal muscle. *Proc. Natl. Acad. Sci. U.S.A.* 97:4380–4385.

Haak, L. L., L. Song, T. F. Molinski, I. N. Pessah, H. Cheng, and J. T. Russell. 2001. Sparks and puffs in oligodendrocyte progenitors: cross talk between Ryanodine receptors and inositol trisphosphate receptors. *J. Neurosci.* 21:3860–3870.

Harris-White, M. E., S. A. Zanotti, S. A. Frautschy, and A. C. Charles. 1998. Spiral intercellular calcium waves in hippocampal slice cultures. *J. Neurosci.* 79:1045–1052.

Horne, J. H., and T. Meyer. 1997. Elementary calcium-release units induced by inositol trisphosphate. *Science.* 276:1690–1693.

Izu, L. T., W. G. Wier, and C. W. Balke. 1998. Theoretical analysis of the Ca^{2+} spark amplitude distribution. *Biophys. J.* 75:1144–1162.

Jiang, Y., M. G. Klein, and M. F. Schneider. 1999. Numerical simulation of Ca^{2+} sparks in skeletal muscle. *Biophys. J.* 77:2333–2357.

Jung, P., and J. W. Shuai. 2001. Optimal sizes of ion channel clusters. *Europhys. Lett.* 56:29–35.

Keizer, J., and G. D. Smith. 1998. Spark-to-wave transition: saltatory transmission of calcium waves in cardiac myocytes. *Biophys. Chem.* 72:87–100.

Keizer, J., G. D. Smith, S. Ponce-Dawson, and J. E. Pearson. 1998. Saltatory propagation of Ca^{2+} waves by Ca^{2+} sparks. *Biophys. J.* 75: 595–600.

Koninck, P. D., and H. Schulman. 1998. Sensitivity of CaM kinase II to the frequency of Ca^{2+} oscillations. *Science.* 279:227–230.

Li, Y., and J. Rinzel. 1994. Equations for $InsP_3$ receptor-mediated $[Ca^{2+}]_i$ oscillations derived from a detailed kinetic model: a Hodgkin-Huxley like formalism. *J. Theor. Biol.* 166:461–473.

Lipp, P., and E. Niggli. 1998. Fundamental calcium release events revealed by two-photon excitation photolysis of caged calcium in guinea-pig cardiac myocytes. *J. Physiol.* 508:801–809.

Mak, D. D., and J. K. Foskett. 1997. Single-channel kinetics, inactivation, and spatial distribution of inositol Trisphosphate (IP_3) receptors in Xenopus oocyte nucleus. *J. Gen. Physiol.* 109:571–587.

Mak, D. D., S. Mcbride, and J. K. Foskett. 2001. ATP-dependent adenophostin activation of inositol 1,4,5-trisphosphate receptor channel gating, kinetic implications for the durations of calcium puffs in cells. *J. Gen. Physiol.* 11:299–314.

Marchant, J., N. Callamaras, and I. Parker. 1999. Initiation of IP_3-mediated Ca^{2+} waves in Xenopus oocytes. *EMBO J.* 19:5285–5299.

Marchant, J. S., and I. Parker. 2001. Role of elementary Ca^{2+} puffs in generating repetitive Ca^{2+} oscillations. *EMBO J.* 20:65–76.

Melamed-Book, N., S. G. Kachalsky, I. Kaiserman, and R. Rahamimoff. 1999. Neuronal calcium sparks and intracellular calcium noise. *Proc. Natl. Acad. Sci. U.S.A.* 26:15217–15221.

Moraru, I. I., E. J. Kaftan, B. E. Ehrlich, and J. Watras. 1999. Regulation of type 1 inositol 1,4,5-trisphosphate-gated calcium channels by $InsP_3$ and calcium: simulation of single channel kinetics based on ligand binding and electrophysiological analysis. *J. Gen. Physiol.* 113: 837–849.

Newman, E. A., and K. R. Zahs. 1997. Calcium waves in retinal glial cells. *Science.* 275:844–847.

Pikovsky, A. S., and J. Kurths. 1997. Coherence resonance in a noise-driven excitable system. *Phys. Rev. Lett.* 78:775–778.

Pratusevich, V. R., and C. W. Balke. 1996. Factors shaping the confocal image of the calcium spark in cardiac muscle cells. *Biophys. J.* 71: 2942–2957.

Rios, E., N. Shirokova, W. G. Kirsch, G. Pizarro, M. D. Stern, H. Cheng, and A. Gonzalez. 2001. A preferred amplitude of calcium sparks in skeletal muscle. *Biophys. J.* 80:169–183.

Roberts, W. M. 1993. Spatial calcium buffering in saccular hair-cells. *Nature.* 363:74–76.

Shuai, J. W., and P. Jung. 2002. Optimal intracellular calcium signaling. *Phys. Rev. Lett.* 88:68102-1–68102-4.

Smith, G. D., J. E. Keizer, M. D. Stern, W. J. Lederer, and H. Cheng. 1998. A simple numerical model of calcium spark formation and detection in cardiac myocytes. *Biophys. J.* 75:15–32.

Strassberg, A. F., and L. J. DeFelice. 1993. Limitations of the Hodgkin-Huxley formalism: effects of single channel kinetics on transmembrane voltage dynamics. *Neural Comp.* 5:843–855.

Sun, X., N. Callamaras, J. S. Marchant, and I. Parker. 1998. A continuum of $InsP_3$-mediated elementary Ca^{2+} signaling events in Xenopus oocytes. *J. Physiol.* 509:67–80.

Swillens, S., G. Dupont, L. Combettes, and P. Champeil. 1999. From calcium blips to calcium puffs: theoretical analysis of the requirements for interchannel communication. *Proc. Natl. Acad. Sci. U.S.A.* 96: 13750–13755.

Thomas, D., P. Lipp, M. J. Berridge, and M. D. Bootman. 1998. Hormone-evoked elementary Ca^{2+} signals are not stereotypic, but reflect activation of different size channel clusters and variable recruitment of channels within a cluster. *J. Biol. Chem.* 273:27130–27136.

Van Kampen, N. G. 1976. Stochastic differential equations. *Physics Reports. Phys. Lett. C.* 24:171–228.